ACS OMEGA

http://pubs.acs.org/journal/acsodf

Article

Effect of Interphase Properties on Isothermal and Non-isothermal Crystallization Behavior of Poly(lactic acid)/Acetylated Starch Blends

Rasool Nasseri, Christine Moresoli,* Aiping Yu, Zhongshun Yuan, and Chunbao Charles Xu

Cite This: *ACS Omega* 2022, 7, 27851−27863

Read Online

ACCESS | Metrics & More | Article Recommendations | Supporting Information

ABSTRACT: The effect of interphase properties on the crystallization behavior of blends of poly(lactic acid) (PLA)/acetylated starch (AS) with different degrees of substitution (DSs) was investigated. Under isothermal crystallization conditions, the rate of crystallization was higher for PLA/DS0.5 and lower for PLA/DS1.5 and PLA/DS2.5 when compared to PLA. In contrast, non-isothermal crystallization behavior indicated a slower rate of crystallization of PLA/DS0.5 and a faster rate of crystallization of PLA/DS1.5 and PLA/DS2.5 compared to PLA at the highest cooling rate (5 °C/min). The potential relationship between crystallization behavior and interphase properties and interphase thickness and formation of rigid amorphous fraction in the interphase, was investigated. The formation of a rigid amorphous fraction in PLA/DS1.5 and a thick interphase in PLA/DS2.5 prevented the formation of crystals on the dispersed phase and interrupted the crystallization under isothermal conditions. Hydrogen bonding in the PLA/DS1.5 blend and hydrophobic interactions in the PLA/DS2.5 blend may facilitate the crystallization at high cooling rates under non-isothermal conditions. Small-angle X-ray scattering analysis revealed the presence of a smaller lamellar structure in PLA/AS blends. The largest amorphous phase among blends was observed for the PLA/DS1.5 blend, which can be attributed to the hydrogen bonding in the interphase region of this blend.

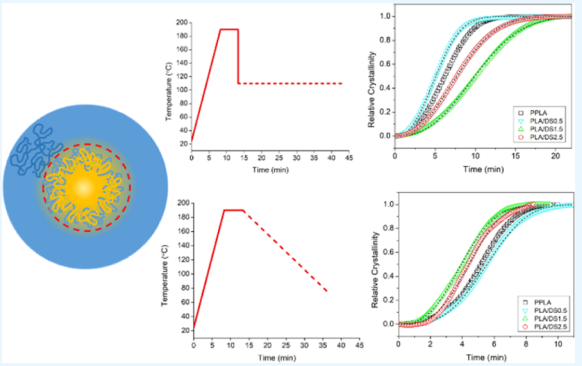

1. INTRODUCTION

Poly(lactic acid) (PLA) has attracted extensive attention because of its biodegradable nature, good mechanical properties, and feedstock renewability.[1,2] Nonetheless, its slow rate of degradation along with its relatively high cost have limited its applications. The blending of PLA with less-expensive biodegradable polymers possessing higher degradation rates can alleviate the limitations of PLA and extend the range of applications. One attractive low-cost biodegradable and renewable polymer is starch.[3] Although starch is an attractive candidate, it has its own limitations. The lack of thermal transition before degradation of starch[4] and its poor compatibility with PLA due to its hydrophilic characteristics limit its application in PLA blends. The limited thermal processability of starch can be improved by plasticization,[4] while the compatibility of starch with PLA can be improved with the use of compatibilizers such as maleic anhydride (MA)[5] and epoxidized soybean oil.[6] The processability and compatibility of starch with PLA can also be obtained by chemical modifications such as butyl etherification, silane modification,[7,8] and acetylation.[9−11]

Crystallization of a material can influence its mechanical and barrier properties and degradation rate. In the context of PLA, increasing the degree of crystallinity can enhance its mechanical properties such as the strength and modulus and can reduce the rate of enzymatic degradation. Higher degree of crystallinity can also improve the barrier properties of PLA.[12] Acetylation of starch that consists of the replacement of the hydroxyl groups in the glucose units with acetyl groups has received limited attention for the development of PLA blends. Despite increasing the compatibility, PLA/acetylated starch (AS) blends were immiscible except for the blend containing fully AS due to thermodynamic considerations.[11] The biphasic microstructure of PLA/AS blends means that the crystallization behavior will be reflected in three regions: the matrix, the dispersed phase, and the interphase (also known as the interfacial region). The addition of a foreign component is known to increase the crystallization rate by increasing the nucleation probability, which is a crucial initial step in the crystallization process.[13] Cai et al.[14] reported on the isothermal crystallization behavior of thermoplastic starch (TPS)/PLA composites. Their results indicated that the crystallization rate and the activation energy of TPS/PLA composites were affected significantly by the incorporation of TPS, which may

Received: January 18, 2022
Accepted: March 22, 2022
Published: August 2, 2022

have acted as a nucleating agent, improving the crystallinity of PLA in TPS/PLA composite materials. The role of TPS as a nucleating agent in improving the crystallinity of PLA in the isothermal crystallization study was also observed in the non-isothermal crystallization study of TPS/PLA conducted by Li et al.[15]

The contributions of the interfacial interactions to the crystallization kinetics remain poorly understood. Interfacial interactions may restrict the movement of the polymer chains in the conformational ordering required for nucleation.[16,17] Alternatively, interfacial interactions may assist with the adsorption of polymer chains in the growth stage of crystallization.[18] Recently, Klonos et al.[19] investigated the effect of polymer filler interfacial interactions on the crystallization behavior of poly(propylene furanoate) comprising graphene oxide (GO) platelets and carbon nanotubes (CNTs). By modification of GO and CNTs, their interfacial interactions with the matrix were increased, decreasing the crystallization rate under isothermal conditions. They attributed the decrease of the isothermal crystallization rate to the formation of a rigid interfacial layer that does not contribute to the crystallization.[19] Wu et al.[20] reported that the incorporation of polystyrene-*b*-polybutadiene-*b*-polystyrene (SBS) accelerated the isothermal melt crystallization of PLA. Compatibilization of the same blend by the poly(styrene-*ran*-methyl acrylate) copolymer decreased the crystallization rate during isothermal crystallization compared to the blend without a compatibilizer.

The purpose of this work was to identify potential relationships between the properties of the interphase, namely, the thickness and chain dynamics, in PLA/AS blends containing AS with different degrees of substitution (DS = 0.5, 1.5, and 2.5) and their isothermal and non-isothermal crystallization behavior. Isothermal crystallization of the PLA/AS blend was investigated by differential scanning calorimetry (DSC) along with Avrami's model, while non-isothermal crystallization of fast-cooled PLA/AS blends was investigated by wide-angle X-ray diffraction (WAXRD), and the effect of the cooling rate on the crystallization kinetics and mechanisms of PLA/AS blends was investigated with DSC and Avrami's model. The thickness of the interphase of the biphasic PLA/AS blends was evaluated with the theoretical approach of Helfand and two experimental methods, small angle X-ray scattering (SAXS) and temperature-modulated DSC (TMDSC). Potential changes in the interactions between the PLA chains and AS associated with the substitution of hydroxyl groups by acetyl groups investigated by Fourier transform infrared (FTIR) spectroscopy analysis and their relationships with the interphase characteristics of the blend will be reported. The impact of DS on the nucleation activity and activation energy of the crystallization of PLA/AS was investigated, and the effect of interfacial interactions on crystallization and the lamellar structure of PLA/AS blends was studied with SAXS.

2. MATERIALS AND METHODS

2.1. Materials. PLA 4032D (M_n = 58 000 g/mol, D-content 1.8%) was provided by NatureWorks Inc. (USA). Corn starch was purchased from local Ontario market (BulkBarn, product code: 000260). Acetylated starch (AS) was produced by mixing corn starch with acetic anhydride at a pre-determined molar ratio of acetic anhydride/starch and acetic acid. The mixture was stirred and heated to 135 °C using a preheated oil bath for 3 h. The reaction mixture was precipitated in a non-solvent, and the precipitate was filtered and washed with a non-solvent to remove any residual acetic acid. The recovered AS products were dried overnight in a vacuum oven at 45 °C to remove any residual solvent. The degree of substitution (DS) represents the number of hydroxyl groups on a glucose unit of starch molecules that are replaced by acetyl groups (from 0 to 3). AS with three DS, 0.5, 1.5, and 2.5, were prepared according to the above procedure.

2.2. Methods. *2.2.1. PLA/AS Blend Preparation.* The details of the PLA/AS blend preparation were as reported previously.[11] To briefly summarize, PLA and AS were dried overnight in a vacuum oven at 80 °C. A lab-scale twin screw extruder (SJSZ-07A, Ruiming Plastics Machinery, Wuhan city, China) was used for the melt-blending of PLA (85 wt %) with AS (15 wt %). The extrusion was performed with a screw speed of 30 rpm at 180 °C for 7 min. The extruded samples were then pelletized. The pellets were then compression-molded using a hot press (PHI, Pasadena Hydraulic Inc., USA) at 200 °C with a pressure of 70 MPa for 4 min to produce thin sheets. The compression-molded samples were cooled rapidly using steel sheets precooled in an ice bath to prepare samples for WAXRD and TMDSC (for thermal transitions). The samples used for the lamellar structure analysis by SAXS were air-cooled slowly. In order to make samples for the interphase studies by SAXS and TMDSC (for interphase thickness), the thin sheets were placed in an oven at 190 °C and quenched with liquid nitrogen to produce completely amorphous blends. A small portion of the quenched sheets was ground to produce a fine powder for FTIR analysis. All samples were stored in a desiccator for further analysis. Table 1 presents the composition and codes of the PLA and PLA/AS blends.

Table 1. Composition, Code, and Processing Time of the PLA and PLA/AS Blends

sample	PLA (wt %)	AS (wt %)	DS of AS
PPLA (processed PLA)	100	0	
PLA/DS0.5	85	15	0.5
PLA/DS1.5	85	15	1.5
PLA/DS2.5	85	15	2.5

2.2.2. Wide-Angle XRD. The crystalline structure of AS and PLA/AS blends was investigated using a wide-angle X-ray diffractometer (D8 FOCUS, Bruker) with Cu Kα_1 radiation and 1.5406 Å wavelength operated at 40 kV and 30 mA. The XRD patterns of AS and PLA/AS blends were recorded in 2θ angle ranges of 3−40 and 10−40, respectively. The step size of the measurements was 0.02°, and the speed was 1 s/step.

2.2.3. Small-Angle X-ray Scattering. SAXS measurements were performed using a SAXSess mc^2 instrument (Anton Paar, Austria) equipped with a Cu Kα X-ray generator with a wavelength (λ) of 0.154 nm, working at a tube current of 50 mA and 40 kV. All measurements were completed at ambient temperature. The scattered X-ray intensity was measured with a 2D charge couple detector located 264.5 mm apart from the sample. The scattering intensity, $I(q)$, measured as a function of the half of the scattering angle, θ, was first desmeared and then corrected for the background absorption and transformed into a plot of scattering intensity versus scattering vector, q ($q = 4\pi \sin \theta/\lambda$), using saxsImage software (Utah SAXS Tools, David P. Goldenberg, September 2012).

2.2.4. Differential Scanning Calorimetry. DSC measurements of PLA and PLA/AS blends were investigated with a

https://doi.org/10.1021/acsomega.2c00360
ACS Omega 2022, 7, 27851−27863

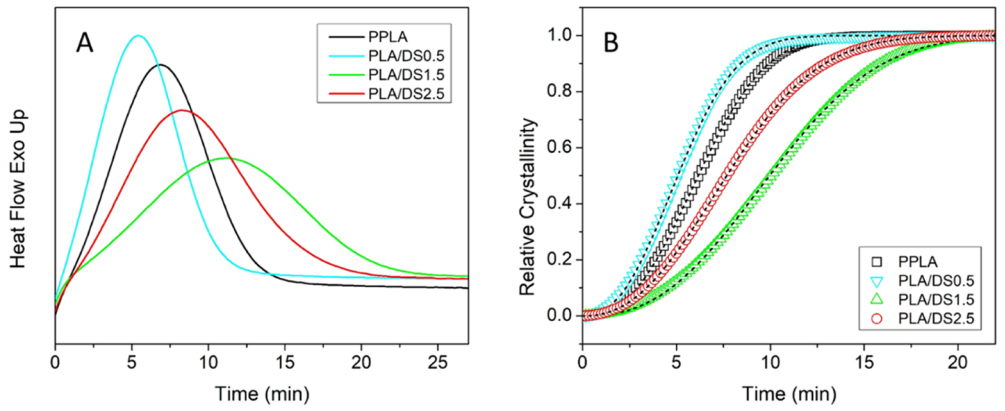

Figure 1. (A) Isothermal crystallization thermograms of PLA and PLA/AS blends obtained at 110 °C, (B) relative crystallinity (χ_t) of PLA and PLA/AS blends according to time. Black-dashed lines show the fitted Avrami equation.

Q2000 TA Instruments (USA) calibrated by indium and sapphire disk standards using standard T_{zero}. Nitrogen with a 50 mL/min flow rate was used as the purge gas. A sample (approximately 10 mg) was placed in an aluminum pan. DSC experiments were conducted with four different thermal procedures:

(a) Isothermal crystallization: heating the sample to 180 °C and maintaining for 5 min to erase the thermal history, followed by cooling to 110 °C and isotherm for 40 min.

(b) Thermal transitions were observed under TMDSC conditions: heating the fast-cooled sample from 40 to 190 °C at a constant heating rate (2 °C/min) coupled with a modulation amplitude of 1.5 °C and a period of 90 s to study the thermal transitions and the initial degree of crystallinity of the blends. The initial degree of crystallinity χ_{c_0} is defined as[21]

$$\chi_{c_0}\,(\%) = \left(\frac{\Delta H_{rev} - \Delta H_{nonrev}}{\Delta H_m^0 \times \delta_{PLA}}\right) \times 100 \quad (1)$$

where ΔH_{rev} and ΔH_{nonrev} are the area under the reversible and non-reversible heat flow, respectively, ΔH_m^0 is the melting enthalpy for 100% crystalline PLA (93.6 J/g[22]), and δ_{PLA} is the mass fraction of PLA in the blends.

The degree of crystallinity χ_c after cold crystallization (exothermic crystallization process occurring on heating) is defined as[8,23]

$$\chi_c\,(\%) = \left(\frac{\Delta H_m}{\Delta H_m^0 \times \delta_{PLA}}\right) \times 100 \quad (2)$$

where ΔH_m is the enthalpy of melting.

(c) Non-isothermal crystallization: heating the sample to 180 °C and maintaining for 5 min to erase the thermal history, followed by cooling at different rates (2, 3.5 and 5 °C/min).

(d) TMDSC for interphase studies: heating to 190 °C at a 20 °C/min heating rate, constant heating at 190 °C for 5 min in order to eliminate thermal history, fast cooling to 40 °C at a 20 °C/min rate to avoid PLA recrystallization, and heating to 70 °C at a 2 °C/min heating rate and an amplitude of 1.5 °C coupled to a 90 s period. Peak deconvolution was obtained with the procedure proposed by Weyer et al.[24] to obtain the in-phase (C') and out-of-phase (C'') components of the heat capacity. A Gaussian peak was fitted to the out-of-phase component of the heat capacity using OriginPro 8.5.

2.2.5. FTIR Spectroscopy. FTIR spectra were recorded on a Tensor-27 Fourier IR spectrometer (Bruker, USA). Samples were prepared by mixing the fine powder of PLA/AS blends with KBr and pressed into KBr pellets. The wave number range was 4000−500 cm^{-1} with a resolution of 1 cm^{-1}. A total of 32 scans were accumulated to reduce spectral noise.

3. RESULTS AND DISCUSSION

Three PLA/AS blends (PLA/DS0.5, PLA/DS1.5, and PLA/DS2.5) with two distinct phases were selected based on our previous work,[11] such that an interphase region exists and the properties of the interphase, namely the thickness and chain dynamics, could be investigated and potentially related to the crystallization behavior.

3.1. Isothermal Crystallization. The isothermal crystallization thermograms of PLA and PLA/AS blends obtained at 110 °C are shown in Figure 1A. The addition of AS affected the crystallization of PLA in the blends. The rate of isothermal crystallization was investigated by analyzing the relative crystallinity (χ_t) at different times (t) calculated as follows

$$\chi_t = \frac{\int_0^t (dH_c/dt)dt}{\int_0^\infty (dH_c/dt)dt} \quad (3)$$

where dH_c/dt is the rate of heat evolution during a given time period. The estimated relative crystallinity, χ_t, presented in Figure 1B, indicates an induction period at the beginning of the crystallization process, which reflects nucleation.[25] The subsequent portion of χ_t as a function of temperature can be represented as a two-step process: primary crystallization (linear portion of χ_t) and secondary crystallization (non-linear portion of χ_t).[14] The first step represents crystal growth until crystals are sufficiently large to touch each other. When crystals touch each other, the second stage starts with the slowing down of the crystallization process.[26] The kinetics of the isothermal crystallization process were investigated with the Avrami model

$$1 - \chi_t = \exp(-Kt^n) \quad (4)$$

where K and n are the crystallization rate constant and the Avrami exponent, respectively. The parameter K gives information on the rate of nucleation and crystal growth. The parameter n provides information on the nucleation

https://doi.org/10.1021/acsomega.2c00360
ACS Omega 2022, 7, 27851−27863

Table 2. Avrami Kinetic Parameters of Processed Pure PLA (PPLA) and PLA/AS Blends for Isothermal Crystallization[a]

sample	n	K (min^{-1})	$t_{1/2}$ (min)	G (min^{-1})	R^2
PPLA	2.51 ± 0.01	0.0072 ± 0.0001	6.16	0.16	0.999
PLA/DS0.5	2.38 ± 0.01	0.0146 ± 0.0002	5.07	0.20	0.999
PLA/DS1.5	2.52 ± 0.01	0.0021 ± 0.0001	9.95	0.10	0.999
PLA/DS2.5	2.31 ± 0.00	0.0062 ± 0.0001	7.68	0.13	1

[a]Reported ranges are 95% confidence intervals on the parameter estimates for the Avrami model.

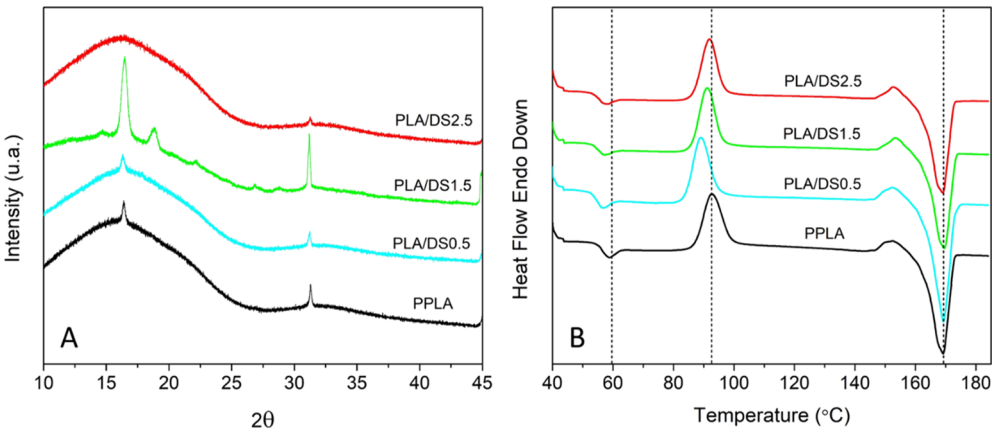

Figure 2. (A) WAXRD diffraction patterns of processed pure PLA (PPLA) and PLA/AS blends according to DS. (B) TMDSC thermograms of PPLA and PLA/AS blends. Dashed lines indicate the major events on the thermograms including glass transition temperature, cold crystallization, and melting.

Table 3. Summary of Thermal Transitions Obtained by TMDSC (Glass Transition Temperature (T_g), Cold Crystallization Temperature (T_c), α' to α Transformation Temperature (T_{cc}), Melting Temperature (T_m), ΔH_{rev} and ΔH_{nonrev} Components of the Heat Flow, Initial Degree of Crystallization (χ_{c_0}) before Cold Crystallization, and Final Degree of Crystallization (χ_c) after Cold Crystallization of Processed Pure PLA (PPLA) and PLA/AS Blends

sample	T_g (°C)	T_c (°C)	T_{cc} (°C)	T_m (°C)	ΔH_{rev} (J/g)	ΔH_{nonrev} (J/g)	χ_{c_0} (%)	χ_c (%)
PPLA	59	92	152	169	8.49	12.52	4.3	38.6
PLA/DS0.5	56	89	152	169	6.82	11.4	5.8	40.1
PLA/DS1.5	57	91	153	169	0.10	10.94	13.6	39.6
PLA/DS2.5	58	92	152	169	10.19	14.73	5.7	41.8

mechanism (simultaneous or sporadic) and the dimensionality of the crystal growth (two or three dimensional) with a typical value between 2 and 4 for PLA crystallization.[27] Large values of n (close to 4) are indicative of sporadic (or combination of sporadic and instantaneous) nucleation with three-dimensional spherulitic growth, while small values of n (close to 2) are attributed to instantaneous (accompanied by some sporadic nucleation) nucleation with two dimensional growth.[12,27]

The Avrami equation provided a very good fit of the relative crystallinity determined experimentally (Figure 1B). The Avrami parameters, n and K, obtained from least square fitting of the experimental data, are presented in Table 2. The Avrami exponent estimates of the PLA/AS blends, reported with 95% confidence interval, were slightly smaller than that of PLA (except for PLA/DS1.5). The addition of AS mildly affected the nucleation mechanism and growth dimensionality of pure PLA. It can be inferred from a slight decrease of the Avrami exponent that the crystal growth in PLA/AS blends (except for PLA/DS1.5) became more two dimensional with more simultaneous nucleation compared to PLA. A slight decrease of the Avrami exponent has been reported previously for PLA/TPS blends (from 2.5 for PLA to 2.3 for the PLA/TPS blend containing 17 wt % TPS).[14]

The Avrami parameters were used to estimate the crystallization half-time ($t_{1/2}$), defined as the time required to reach 50% relative crystallinity (eq 5), and the crystallization rate (G) was given as the reciprocal of $t_{1/2}$ (eq 6).

$$t_{1/2} = \left(\frac{\ln 2}{K}\right)^{1/n} \tag{5}$$

$$G = 1/t_{1/2} \tag{6}$$

Two distinct types of $t_{1/2}$ were estimated translating in a higher rate of crystallization for PLA/DS0.5 ($t_{1/2}$ = 5.07 min) and a slower rate of crystallization for PLA/DS1.5 ($t_{1/2}$ = 9.95 min) and PLA/DS2.5 ($t_{1/2}$ = 7.68 min) compared to PPLA ($t_{1/2}$ = 6.16 min).

3.2. Thermal Transition and Crystallization during Non-isothermal Crystallization. Non-isothermal crystallization conditions are more representative of industrial polymer processing, specifically the crystallization taking place in the cooling phase. In order to investigate the crystallization under non-isothermal conditions, two sets of experiments were

https://doi.org/10.1021/acsomega.2c00360
ACS Omega 2022, 7, 27851−27863

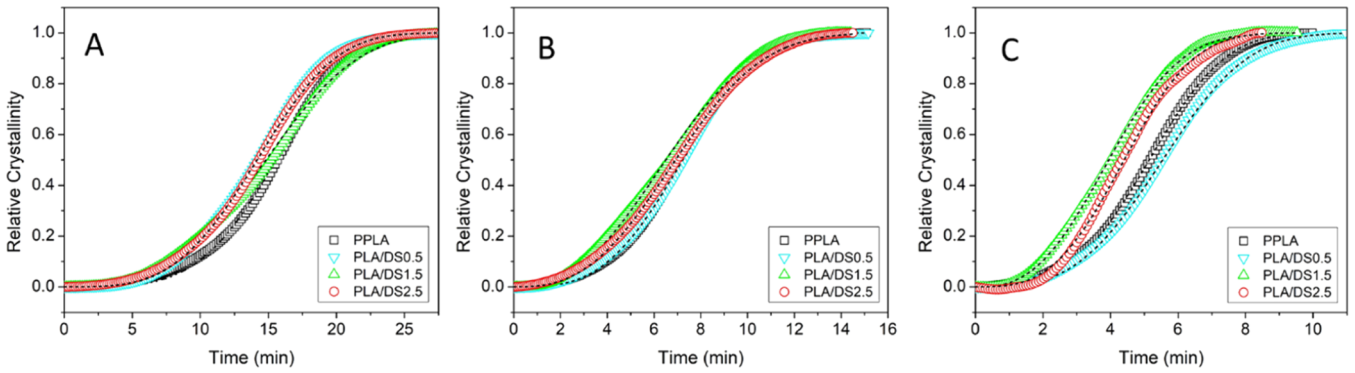

Figure 3. Relative crystallinity of PPLA and PLA/AS blends at different cooling rates: (A) 2, (B) 3.5, and (C) 5 °C/min. Black-dashed lines represent the fitted adjusted Avrami equation.

conducted. The first set of experiments investigated the effect of fast cooling on the properties of compression-molded samples by cooling them very rapidly using steel sheets precooled in an ice bath. The crystalline structure and level of crystallinity of the blends after fast cooling were investigated by WAXRD and TMDSC. Figure 2A shows the XRD patterns of fast-cooled PLA/AS blends. A very low level of crystallinity was observed in all blends except for PLA/DS1.5, most probably due to the fast cooling. The diffraction peak at $2\theta = 31°$ from the (1010) plane of the α-form crystal[28] was observed for all blends. The peak at $2\theta = 16.5°$, representing the diffraction from (110) and/or (200) planes of the disordered α'-form,[29] was observed for all blends except PLA/DS2.5. The PLA/DS1.5 blend has the highest degree of crystallinity and distinct diffraction patterns such as a peak at $2\theta = 19°$ from the (203) plane of the α-form crystal.[30]

The influence of AS on the thermal transitions of fast-cooled PLA/AS blends investigated by TMDSC is presented in Figure 2B. The glass transition temperature (T_g) of PPLA decreased by a few degrees with the incorporation of AS due to the plasticization effect (Table 3). The small peak in the T_g region (pointed out by a dashed line) of the TMDSC thermograms showed that the glass transition included an enthalpy relaxation.[31] Cold crystallization, an exothermic process occurring during heating (exothermic peak (T_c) around 90 °C) was observed for all samples. A second exothermic peak (T_{cc}) was observed prior to the melting temperature (T_m) and was attributed to the crystal transformation from the disordered α' form crystal to the more ordered α form crystal.[29] The initial degree of crystallinity before cold crystallization (χ_{c_0}) was estimated by deconvolution of the heat flow in its reversible and non-reversible parts (eq 1). An example of the deconvolution of the total heat flow for PPLA is presented in the Supporting Information, Figure S1. The estimated initial degree of crystallinity (χ_{c_0}) is presented in Table 3. The PLA/DS1.5 blend had the highest initial degree of crystallinity that is supported by the WAXRD results (Figure 2A) and will be discussed later. The final degree of crystallinity after cold crystallization (χ_c) was similar for all blends and slightly higher than that of PPLA. All blends reached the same level of crystallinity after cold crystallization.

The second set of experiments investigated the non-isothermal crystallization of PPLA and PLA/AS blends in DSC experiments at three different cooling rates of 2, 3.5, and 5 °C/min. The thermograms were analyzed with the Avrami equation modified to account for the non-isothermal conditions, where the effect of the cooling rate (β) is captured in the crystallization rate constant K_c[32]

$$\ln K_c = \frac{\ln K}{\beta} \tag{7}$$

where K_c is the rate constant for non-isothermal crystallization.

The relative crystallinity (χ_t), estimated with eq 3, over time and the fitted adjusted Avrami equation (eq 4 with K-substituted by K_c) according to the cooling rate for PPLA and PLA/AS blends are depicted in Figure 3A–C, and the Avrami parameters, n and K_c, obtained by least square fitting are presented in Table S1. The Avrami exponent n for the non-isothermal crystallization generally decreased with increasing cooling rate, indicating a decrease in the dimensionality of the crystal growth while nucleation becomes more instantaneous.

At the lowest cooling rate, 2 °C/min, $t_{1/2}$ was about 15 min for PPLA, and all PLA/AS blends indicate a similar crystallization rate, which reflects the overlapping of relative crystallinity versus time curves (Figure 3A). Differences in the relative crystallinity versus time between PPLA and the PLA/AS blends appeared at a 3.5 °C/min cooling rate. Distinct differences in the relative crystallinity were observed at the highest cooling rate, 5 °C/min, with slower crystallization for the PLA/DS0.5 blend, while faster crystallization was observed for PLA/DS1.5 and PLA/DS2.5 compared to PPLA. This in contrast to the isothermal crystallization conditions, where the PLA/DS1.5 blend showed the slowest rate of crystallization in isothermal crystallization but the non-isothermal crystallization behavior may explain the highest initial degree of crystallinity for this sample observed in WAXRD (Figure 2A) and TMSDC (Table 3) experiments.

The exothermic peak of crystallization of PPLA and PLA/AS blends at different cooling rates (Figure S2) shows that the peak of the crystallization temperature (T_p) shifted to lower temperatures as the cooling rate increased for all blends except the PLA/DS1.5 blend, where T_p shifted to higher temperatures with increasing cooling rate, Table 4. The formation of a rigid amorphous region with a slower dynamic around the dispersed phase in PLA/DS1.5 explains the shift of T_p to higher temperatures. Polymer chains in this region require a higher energy content for conformational ordering to start the nucleation. Details of the formation of this region will be discussed later.

The activation energy of non-isothermal crystallization was estimated using an advanced isoconversional method proposed by Vyazovkin.[33] Because this method assumes that the reaction model is independent of the cooling rate, activation energy of

https://doi.org/10.1021/acsomega.2c00360
ACS Omega 2022, 7, 27851−27863

Table 4. Nucleation Activity Parameters of PPLA and PLA/AS Blends during Non-isothermal Crystallization

sample	β (°C/min)	T_p (°C)	B or B^* (K^2)	ϕ_n
PPLA	2	99.15	37 403	
	3.5	95.53		
	5	95.49		
PLA/DS0.5	2	102.32	22 170	0.59
	3.5	97.57		
	5	95.45		
PLA/DS1.5	2	99.62	−47 851	−1.28
	3.5	101.81		
	5	102.49		
PLA/DS2.5	2	99.48	164 263	4.39
	3.5	98.72		
	5	98.68		

crystallization at each value of relative crystallinity ($E_a(\chi_t)$) is also independent of the cooling rate. Therefore, by minimization of $\Phi(E_a(\chi_t))$, $E_a(\chi_t)$ can be determined

$$\Phi(E_a(\chi_t)) = \sum_{i=1}^{n} \sum_{j\neq i}^{n} \frac{J[E_a(\chi_t), T_i(\chi_t)]}{J[E_a(\chi_t), T_j(\chi_t)]} \tag{8}$$

$$J[E_a(\chi_t), T_i(\chi_t)] = \frac{1}{\beta_i} \int_{T_0}^{T_{\chi_t}} \exp\left[\frac{E_a(\chi_t)}{RT_i(\chi_t)}\right] dT \tag{9}$$

where J is the Arrhenius integral, i and j represent the different cooling rates, and R is the universal gas constant. The activation energy values of crystallization at each value of relative crystallinity ($E_a(\chi_t)$) for PPLA and PLA/AS blends are presented in Figure 4A. The activation energy of crystallization is initially high at the beginning of the crystallization (low values of relative crystallinity (χ_t)), where the temperature is high due to the limited nucleation. As crystallization proceeds, the activation decreases reflecting the increased relative crystallinity (χ_t) and the facile nucleation. The activation energy of PLA/DS0.5 was lower than the activation energy of PPLA in the entire range of χ_t, while the activation energy of the PLA/DS1.5 and PLA/2.5 blends was higher than that of PPLA in the entire range of χ_t.

The nucleation activity of AS in PLA was assessed by following the method suggested by Dobreva and Gutzow[34] for polymer blends, where the dispersed component (ϕ_n), defined as a factor by which the required energy for crystallization of the matrix decreases, can be calculated using

$$\phi_n = \frac{B^*}{B} \tag{10}$$

where B^* and B are parameters related to the polymer blend (PLA/AS) and the pure polymer (PLA), respectively, and can be calculated with the following equations

$$\ln(\beta) = C_1 - \frac{B^*}{\Delta T_p^2} \tag{11}$$

$$\ln(\beta) = C_2 - \frac{B}{\Delta T_p^2} \tag{12}$$

where β is the cooling rate, C_1 and C_2 are constants, and $\Delta T_p = T_m - T_p$ is the supercooling. B and B^* are estimated from the slope of the plot $\ln(\beta)$ versus $1/\Delta T_p^2$ (Figure 4B). The estimated nucleation activity for PLA/AS blends is presented in Table 4. When the dispersed component in a blend is extremely active for nucleation, ϕ_n approaches 0, while for the inert dispersed component, it is about 1. A nucleation activity higher than 1 can be interpreted as an antinucleating effect.[13] This study showed that AS had a wide range of nucleation activity for PLA. The blend containing AS DS0.5 showed some nucleation activity, while the blend containing AS DS2.5 displayed an antinucleating effect. An unusual nucleation activity was observed for AS DS1.5, where the nucleation activity was negative. The formation of a rigid amorphous region with a slower dynamic around the dispersed phase in PLA/DS1.5 explains this unusual nucleation activity. Details of the formation of this region will be discussed later.

To better understand the relationships between crystallization kinetics of AS as the dispersed phase in PLA/AS blends, properties of the interphase, the thickness of the interphase, dynamics of the PLA chains in the interphase, and interfacial interactions were studied. Interfacial diffusion and interactions may restrict the movement of the PLA chains in the conformational ordering required for nucleation. Alternatively, interfacial interactions may assist with the adsorption of PLA chains in the growth stage of crystallization.

3.3. Thickness of the Interphase. The thickness of the interphase for biphasic PLA/AS blends according to DS was estimated theoretically and experimentally using two methods

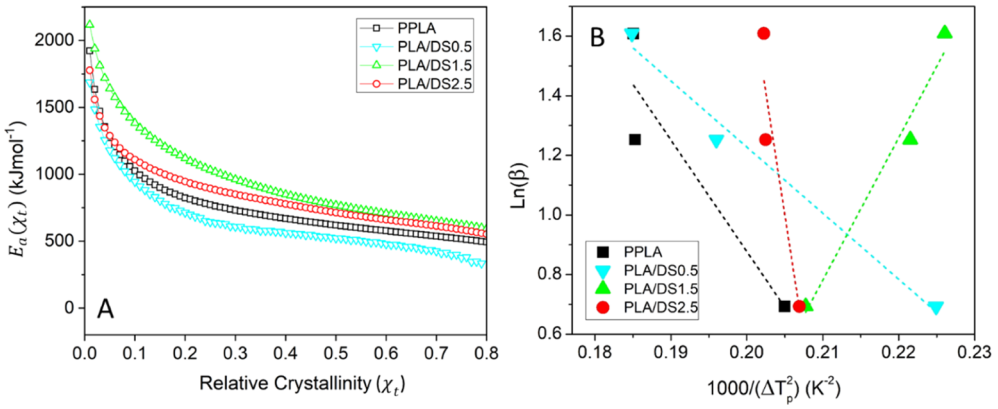

Figure 4. (A) Activation energy of crystallization according to relative crystallinity of PPLA and PLA/AS blends during non-isothermal crystallization. (B) Nucleation activity plots of PPLA and PLA/AS blends.

https://doi.org/10.1021/acsomega.2c00360
ACS Omega 2022, 7, 27851−27863

Table 5. Properties of PLA and AS

material	ρ_i (g cm^{-3})	α_i (10^{-4} K^{-1})	$\delta_i(298)$ (J cm^{-3})$^{1/2}$	M_i (g mol^{-1})	molecular weight (g mol^{-1})	b_i (nm)
PLA	1.25[a]	7.4[a]	21.73[b]	76	58 000	0.72[c]
DS0.5	1.46	0.67	37.21	183	19 200	2.4[d]
DS1.5	1.40	1.82	29.12	225	3 500 000	2.4[d]
DS2.5	1.36	2.24	24.38	267	1 800 000	2.4[d]

[a]Reference 42. [b]Reference 43. [c]Reference 44. [d]References 45 and 46

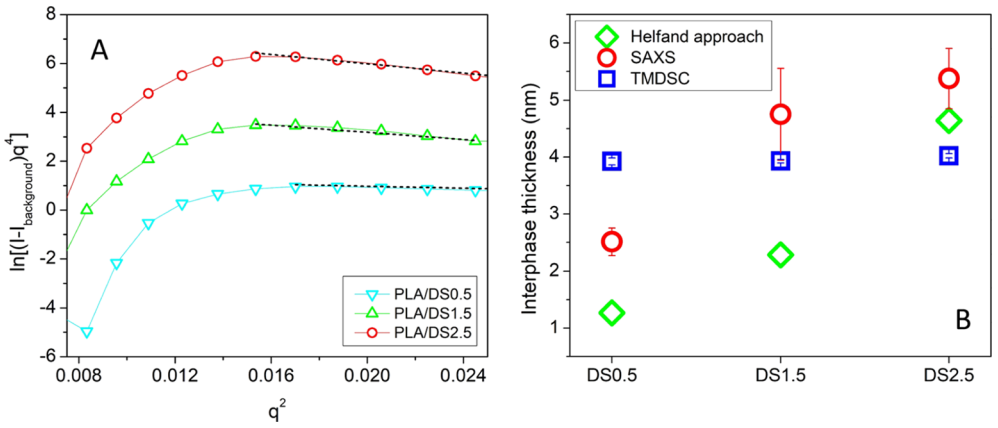

Figure 5. (A) Porod plots of PLA/AS blends at room temperature. The plots are shifted vertically for better visualization. The slope of the dashed black lines were used to estimate the thickness of the interphase. (B) Thickness of the interphase of PLA/AS blends according to DS and estimated using three methods (theoretical calculation, SAXS, and TMDSC). The error bars are taken from the deviation in the linear fit of $\ln[(I - I_{background})q^4]$ versus q^2 for the SAXS measurements and are taken from the deviation in the Gaussian peak fit for the TMDSC measurements and represent 95% confidence interval.

(SAXS and TMDSC), representing three independent methods.

The theoretical estimation of the thickness was based on the approach proposed by Helfand and Tagami and properties of the pure components.[35−38] In this approach, the thickness of the interphase ($a_{I\infty}$) is related to the interaction parameter by the lattice model considering the infinite chain length

$$a_{I\infty} = 2\left[\frac{\beta_A^2 + \beta_B^2}{2\chi_{AB}(\rho_{0A}\rho_{0B})^{1/2}}\right]^{1/2} \quad (13)$$

with

$$\beta_i^2 = \frac{\rho_{0i} b_i^2}{6} \quad (14)$$

where χ_{AB} is the Flory−Huggins interaction parameter, b_i is the Kuhn segment length, and $\rho_{0,i}$ is the segment density of component i (considered equal to the density of component i). The subscript A and B represent PLA and AS, respectively. The thickness of the interphase was corrected to account for entropic effects as suggested by Broseta et al.[39] with an expression that goes beyond the approximation of infinite molecular weight

$$a_I = a_{I\infty}[1 + (1/\omega_A + 1/\omega_B)\ln 2] \quad (15)$$

where $\omega_i = \chi_{AB}N_i$ is the degree of incompatibility and N_i is the number of segments of component i, estimated as N_i = molecular weight/M_i. Kong et al.[40] combined the interaction energy of the Flory−Huggins theory with the CRS model[41] to develop a modified Flory−Huggins interaction parameter that was used in eq 13 as follows

$$\chi_{AB} = \frac{v}{k_B T}(\tilde{\rho}_A \delta_{A,0} - \tilde{\rho}_B \delta_{B,0})^2 \quad (16)$$

where $\tilde{\rho}_i$ and $\delta_{i,0}$ are the reduced density and the reduced solubility parameters at 0 K of component i, respectively, and k_B is the Boltzmann constant. The parameter v is the geometric average of the segment volumes for the pure components

$$v = \sqrt{v_A v_B} \quad (17)$$

The volume of the hard core segment was defined as

$$v_i = M_i/N_{Av}\rho_i^* \quad (18)$$

M_i is the monomer (repeating unit) molecular weight and N_{Av} is Avogadro's number. The hard core density ρ_i^* is calculated from the density at temperature T with the following relation

$$\rho_i^* = \rho_i(T)\exp(\alpha_i T) \quad (19)$$

where α_i is the volumetric thermal expansion coefficient. Reduced density at temperature T was estimated from the hard core density and the density at temperature T

$$\tilde{\rho}_i(T) = \rho_i/\rho_i^* \quad (20)$$

The parameter $\delta_{i,0}$ was calculated from the reduced solubility parameters and the reduced density at 298 K and used to estimate χ_{AB} in eq 16

$$\delta_{i,0}^2 = \delta_i^2(298)/\tilde{\rho}_i(298) \quad (21)$$

The pure component properties of AS were experimentally measured and reported previously,[11] while the pure component properties of PLA were obtained from the literature and are summarized in Table 5.

https://doi.org/10.1021/acsomega.2c00360
ACS Omega 2022, 7, 27851−27863

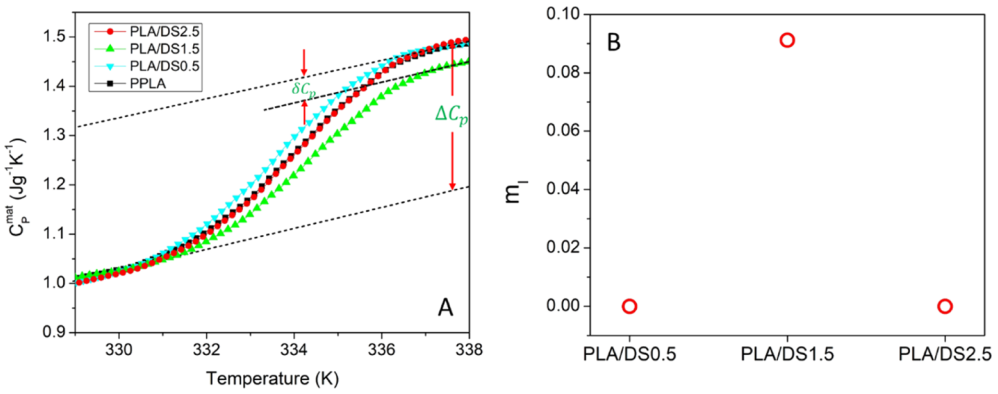

Figure 6. (A) Normalized specific heat capacity of the matrix for PLA/AS blends. The curves are vertically shifted to align at lower temperatures below T_g and to illustrate the change in jump of specific heat capacity at the glass transition temperature. The dotted lines are presented to guide the eye. The specific heat capacity of the interphase (δC_p) is defined as the differences of the specific heat capacity jump at T_g between pure PLA and the PLA matrix in the PLA/AS blends: $\delta C_p = \Delta C_p\text{-}\Delta C_p^{mat}$. (B) Weight fraction of the PLA matrix with slower dynamics (RAF).

In the SAXS method, the interphase thickness (a_I) estimates relied on Porod's analysis. The original Porod's law, initially developed for an ideal two-phase system with a sharp boundary between the two phases and the absence of background effect, was modified to handle real polymer systems. First, the scattering intensity was corrected for the effect of thermal density fluctuations.[47] Second, the effect of diffuse interface boundary (interphase) was accounted as proposed by Vonk[48] and Ruland.[49] The scattered intensity was expressed as

$$I(q) - I_{background} = \frac{K_p}{q^4} \exp(-4\pi^2\sigma^2q^2) \quad (22)$$

where K_p is a constant and $\exp(-4\pi^2\sigma^2q^2)$ is the Gaussian smoothing function that corrects the negative deviations from Porod's law as a result of an interface, with standard deviation of σ. After plotting $\ln[(I - I_{background})q^4]$ versus q^2, σ is estimated from the slope of the resulting lines at large scattering vectors (Figure 5A). The interphase thickness was then estimated as $a_I = 12^{1/2}\sigma$. The parameter $I_{background}$ was calculated from the slope of a plot of $q^4I(q)$ versus q^4 at large qs.

In the TMDSC method, the interphase thickness estimates were based on the measured temperature fluctuation of the amorphous regions combined with Donth's approach. In this approach, the characteristic length scale (ξ_a) of the dynamic heterogeneities is associated with the volume of a CRR (V_a)[50] and can be calculated as follows

$$V_a = \xi_a^3 = \frac{\Delta(C_p^{-1})k_BT_a^2}{\rho(\delta T)^2} \quad (23)$$

where $\Delta(C_p^{-1})$ is the change of the inverse heat capacity between the liquid and the glass states, k_B is the Boltzmann constant, and ρ is the density of the amorphous phase. When the out-of-phase component of the heat capacity, $C''(T)$, is fitted by a Gaussian peak, δT corresponds to the standard deviation of this Gaussian peak (δT = full width at half maximum/2.35) and T_a corresponds to the temperature at the maximum of the Gaussian peak (Table S2, Supporting Information).

The theoretical (Helfand approach) and the experimental TMDSC and SAXS estimates of the interphase thickness for biphasic PLA/AS blends according to DS are presented in Figure 5B. Estimates of the interphase thickness differed according to the method and the DS of AS.

The theoretical and SAXS interphase thickness estimates increased with increasing DS. The theoretical interphase thickness estimates are generally lower than those deduced from the SAXS experimental measurements. These differences may reflect the underlying assumptions and approximations of the theoretical calculations, namely: (i) thermodynamic equilibrium conditions that may be far from the actual processing conditions due to the kinetic limitations of the system; (ii) the use of pure component properties for the estimation of the Flory−Huggins interaction parameter; and (iii) the use of the properties of amylose for the calculation of the Kuhn segment length while AS contains amylose and amylopectin and AS with different DS possesses different chain flexibility due to the replacement of the hydroxyl groups with acetyl groups.

The interphase thickness estimated by TMDSC showed a negligible effect of the DS of the AS (Table S2,Supporting Information). These estimates may reflect the low sensitivity of the TMDSC method in capturing the effect of DS from heat flow characteristics.

In polymer blends, the thermodynamic affinity (χ_{AB}) and the Kuhn segment length of the components (a measure of chain stiffness, $b \propto \sqrt{C_\infty}$) are the primary contributors in the interphase thickness estimation (eq 1). In contrast, previous studies on polymer nanocomposite materials indicate that the chain stiffness predominates, while the thermodynamic affinity has a negligible effect on the thickness of the interfacial layer.[51,52] It is the characteristic ratio (C_∞, chain stiffness) of the matrix that was shown to be the main contributing factor in these systems.[53]

The role of the interfacial interactions in the interphase thickness for the PLA/AS blends investigated in this study will be discussed in the next sections by evaluating the change of the specific heat capacity at the glass transition temperature as a means to provide information on the fraction of the chains of the matrix contributing to the glass transition and from FTIR analysis.

3.4. Dynamics of the Interphase. The dynamics of the interphase are known to be strongly influenced by the interactions between the chains of the matrix and the dispersed phase.[54] In the PLA/AS blends investigated in this study, the interactions between the PLA matrix and the AS dispersed

https://doi.org/10.1021/acsomega.2c00360
ACS Omega 2022, 7, 27851−27863

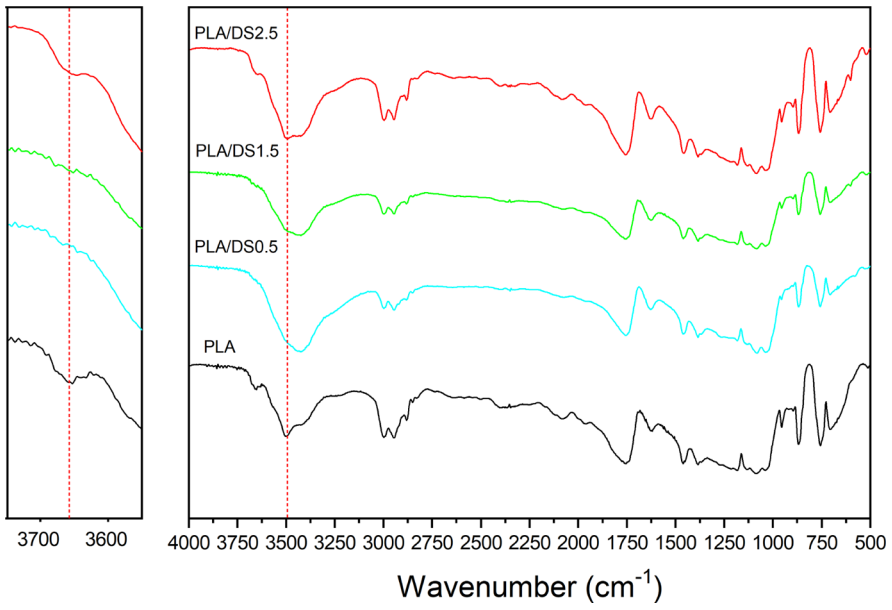

Figure 7. FTIR spectra of PLA and PLA/AS blends. One region of spectra is enlarged: 3550 to 3750 cm^{-1} (left hand side).

phase are expected to be influenced by the DS of the AS, namely the hydroxyl and acetyl contents. These interactions were investigated by examining the behavior of the specific heat capacity at the glass transition temperature as a means to provide information on the fraction of the chains of the matrix contributing to the glass transition. By comparing the behavior of the PLA matrix in the blends to that of pure PLA, one can estimate the fraction of the chains of PLA in the matrix that has slower dynamics due to its interactions with the AS dispersed phase and that do not contribute to the glass transition [rigid amorphous fraction (RAF)].[55] This approach has been used previously for polymer nanocomposites[53,54] but not for polymer blends, where the dispersed phase is significantly larger than that in nanocomposite materials. We have used TMDSC to investigate these effects in PLA/AS blends by accurately estimating the heat capacity while avoiding kinetic effects such as solvent evaporation, crystallization, and enthalpic recovery.[54] The normalized heat capacity of the PLA matrix in the PLA/AS blends (C_p^{mat}) can be calculated as

$$C_p^{mat} = \frac{C_p^{blend} - C_p^{AS} m_{AS}}{1 - m_{AS}} \quad (24)$$

where C_p^{blend} and C_p^{AS} are the specific heat capacity of the blend and AS (Figure S3) and m_{AS} is the weight fraction of AS in the blend. Figure 6A depicts the normalized specific heat capacity of the PLA/AS blends and pure PLA. A lower increase of specific heat capacity at glass transition can be observed for PLA/DS1.5 compared to pure PLA and the other blends due to the lower fraction of the matrix chains contributing to the glass transition in these samples. The specific heat capacity of the interphase (δC_p), defined as the difference between the specific heat capacity increment at T_g of pure PLA (ΔC_p) and the PLA matrix in the blends (ΔC_p^{mat}), $\delta C_p = \Delta C_p - \Delta C_p^{mat}$, was used to estimate the weight fraction of the PLA matrix in the blends with slower dynamics (m_I) or so-called RAF as follows

$$m_I = \frac{\delta C_p}{\Delta C_p} \quad (25)$$

The calculated m_I for the biphasic PLA/AS blends (Figure 6B) indicates that a portion of the PLA matrix has slower dynamics ($m_I \neq 0$) for the PLA/DS1.5 blend, while no fraction with slower dynamics was estimated for the PLA/DS0.5 and PLA/DS2.5 blends ($m_I = 0$). The differences of m_I estimates according to DS indicate the lack of correlation between the level of interfacial interactions and the interphase thickness (Figure 6B) in PLA/AS blends. The PLA/DS1.5 blend has a lower interphase thickness compared to PLA/DS2.5, but a much higher level of interfacial interactions according to their m_I estimates. Some authors have attempted to calculate the interphase thickness by the weight fraction of the matrix in the blends with slower dynamics, considering a similar density for the matrix and the interphase,[53] but recent studies show that the density of the interphase can be different than the matrix depending on the interfacial interactions.[56] The lack of correlation between the interphase thickness and interfacial interactions has been reported previously for polymer nanocomposites.[51,52]

3.5. FTIR Analysis of the Interfacial Interactions. Further analysis of the interactions taking place at the interface between the PLA matrix and the AS dispersed phase in PLA/AS blends was carried out using FTIR spectroscopy (Figure 7).

The FTIR spectra of PLA and the PLA/AS blends are similar to each other except for a region marked with a dashed line. This is the region of −OH stretching. Three peaks were observed in the PLA spectrum. The first peak is broad and appears at 3446 cm^{-1} that can be associated with ν(C−O···H).[57] The second and third peaks, occurring at 3506 and 3653 cm^{-1}, are located in the region of the free −OH stretching.[57] The disappearance of these peaks in PLA/DS0.5 and PLA/DS1.5 blends indicates a higher level of hydrogen bonding compared to the PLA/DS2.5 blend and could reflect the higher hydroxyl group per repeating unit in DS0.5 and DS1.5. This may explain the weight fraction of the PLA matrix with slower dynamics estimated for the PLA/DS1.5 blend. The

https://doi.org/10.1021/acsomega.2c00360
ACS Omega 2022, 7, 27851−27863

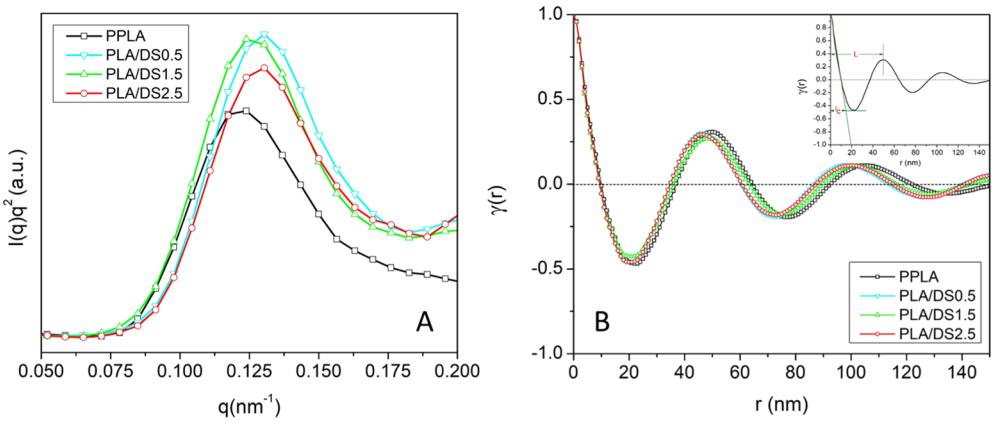

Figure 8. (A) Lorentz-corrected SAXS profiles recorded at room temperature for PPLA and PLA/AS blends. (B) One-dimensional correlation functions of PLA and PLA/AS blends.

diffusion between the matrix and the dispersed phase and the hydrogen bonding between the two phases could lead to an interphase with slower dynamics. Due to the limited diffusion of PLA in AS in PLA/DS0.5 blend, the hydrogen bonding did not lead to the slowdown of the dynamics. The absence of slowdown in the dynamics for PLA/DS2.5 suggests that the diffusion of PLA in AS was not sufficient to alter the dynamics in the interphase region for this blend. In contrast, strong physical interactions such as hydrogen bonds may have contributed to the slower dynamics in the interphase region for the PLA/DS1.5 blend.

It is now possible to relate the isothermal and non-isothermal crystallization behavior of PLA/AS blends to their interphase properties. The PLA/DS0.5 blend showed faster isothermal crystallization compared to PPLA, while the PLA/DS1.5 and PLA/DS2.5 blends presented slower isothermal crystallization compared to PPLA. Diffusion of PLA in AS in the interphase region in PLA/AS blends prevents the formation of crystals on the dispersed phase in the PLA/DS1.5 and PLA/DS2.5 blends. Due to the limited diffusion of PLA in AS and no RAF in the PLA/DS0.5 blend, the dispersed phase can act as the nucleating agent to facilitate the crystallization. In non-isothermal crystallization, this trend is opposite. At the highest cooling rate, slower crystallization compared to PPLA was observed for the PLA/DS0.5 blend, while PLA/DS1.5 and PLA/DS2.5 showed faster crystallization compared to PPLA. The PLA/DS1.5 blend showed the highest rate of crystallization at the highest cooling rate, while in isothermal crystallization this blend showed the slowest rate of crystallization. Hydrophobic interactions and hydrogen bonging between PLA and AS in the PLA/DS1.5 and PLA/DS2.5 blends appeared to facilitate the crystallization at high cooling rates.

Formation of a RAF in PLA/DS1.5 and the diffusion of PLA in AS and in PLA/DS2.5 may also explain the higher activation energies of these two blends compared to PPLA. The highest activation energy was observed for the PLA/DS1.5 blend (769 kJ mol^{-1} at χ_t = 0.5), while the lowest activation energy was observed for the PLA/DS0.5 blend (521 kJ mol^{-1} at χ_t = 0.5).

The PLA/AS blends investigated in this study showed that AS had a wide range of nucleation activities. The blend containing AS DS0.5 showed some nucleation activity, while the blend containing AS DS2.5 displayed an antinucleating effect, Table 4. A thick interphase between PLA and AS in the PLA/DS2.5 blend as the result of the diffusion of PLA in AS may explain the antinucleating effect of AS DS2.5. An unusual nucleation activity was observed for AS DS1.5, where the nucleation activity was negative, Table 4. The nucleating activity of AS DS1.5 may reflect the formation of a RAF around the dispersed phase in the PLA/DS1.5 blend.

3.6. Lamellar Structure of PLA and PLA/AS Blends.

The lamellar structure of PLA and PLA/AS blends was investigated by SAXS. To prepare the samples for this experiment, hot-pressed films were cooled down slowly at room temperature in a non-isothermal manner to ensure the formation of the crystalline structure. The Lorentz-corrected SAXS data are presented in Figure 8A as Iq^2 versus q, where $q = 4\pi/\lambda \sin(\theta)$ and θ and λ are half of the scattering angles and wavelength of X-ray, respectively.

The morphological parameters of the lamellar structure including the long period, the average lamellar thickness, and the amorphous-phase thickness were estimated from the normalized one-dimensional correlation function calculated from the scattered intensity by using the following equation[58]

$$\gamma(r) = \frac{\int_0^\infty I(q)q^2 \cos(qr)\mathrm{d}q}{\int_0^\infty I(q)q^2\mathrm{d}q} \quad (26)$$

where r is the direction along which the electron density distribution was measured.

The data were extended from the smallest measured q to zero by linear extrapolation. Large q values were decayed to infinite q using Porod's law (q^{-4} decay).[47] The average long period (L) was estimated from the first maximum of the correlation function. The average lamellar thickness (l_c) was determined from the r-axis value of the intersection point between the tangent-line at $\gamma(r) = 0$ and the tangent-line at the first minimum in the correlation curve as shown in the inset of Figure 8B. The thickness of the amorphous phase (l_a) was calculated from L and l_c ($l_a = L - l_c$).[58] The long period can also be estimated from equation $L = 2\pi/q^*$, where q^* is the peak of the Lorentz-corrected plot.[47] The normalized one-dimensional correlation functions of PLA and PLA/AS blends are plotted in Figure 8B.

The morphological parameters of the lamellar structure presented in Table 6 indicate lower L, l_c, and l_a estimates for all PLA/AS blends compared to PPLA. The PLA/DS1.5 blend displayed the most similar L and l_a parameters to those of PLA. During the crystallization process, the crystallization of the PLA chains will be competing with the interactions between

https://doi.org/10.1021/acsomega.2c00360
ACS Omega 2022, 7, 27851−27863

Table 6. Morphological Parameters of the Lamellar Structure of PPLA and PLA/AS Blends Obtained by SAXS

	L (nm)			
sample	peak of Lorentz-corrected plot	correlation function	l_c (nm)	l_a (nm)
PPLA	50.7	49.9	15.2	34.7
PLA/DS0.5	48.2	46.3	14.2	32.1
PLA/DS1.5	50.7	48.1	14.1	34
PLA/DS2.5	48.2	46.3	14.3	32

the PLA and AS chains. This competition will influence the final lamellar structure of the material.[59] The interactions between the PLA and the AS chains will interfere with the conformational changes of the PLA chains that are required for crystallization to occur and which would lead to a smaller lamellar structure. With this in mind, the higher thickness of the amorphous phase (l_a) of the PLA/DS1.5 blend may be attributed to the hydrogen bonding between the PLA and AS components in this blend.

4. CONCLUSIONS

The role of the degree of acetylation of starch and the interphase properties in the crystallization characteristics of PLA/AS blends was investigated under isothermal and non-isothermal crystallization conditions. The faster rate of crystallization compared to PLA was observed for the PLA/DS0.5 blend under isothermal crystallization conditions. The PLA/DS1.5 and PLA/DS2.5 blends showed a lower rate of crystallization compared to PLA under isothermal crystallization conditions. The formation of a RAF in PLA/DS1.5 and a thick interphase in PLA/DS2.5 prevented the formation of crystals on the dispersed phase and interrupted the crystallization. In contrast to the isothermal crystallization conditions, a slower rate of crystallization was observed for the PLA/AS0.5 compared to PLA, while the crystallization rate of the PLA/DS1.5 and PLA/DS2.5 was higher than that of PLA at the highest rate of cooling (5 °C/min) under non-isothermal conditions. Hydrogen bonding in the PLA/DS1.5 blend and hydrophobic interactions in the PLA/DS2.5 blend may facilitate the crystallization at high cooling rates. The lamellar structure of the PLA/AS blends deduced from SAXS experiments indicated a smaller lamellar structure for all the PLA/AS blends compared to pure PLA. The largest amorphous phase was observed for the PLA/DS1.5 blend due to the presence of significant interfacial hydrogen bonding, which interferes with the conformational changes required for crystallization.

ASSOCIATED CONTENT

Supporting Information

The Supporting Information is available free of charge at https://pubs.acs.org/doi/10.1021/acsomega.2c00360.

Example of peak deconvolution of the total heat flow to its reversible and non-reversible components for PPLA; adjusted Avrami kinetic parameters of PPLA and PLA/AS blends during non-isothermal crystallization; exothermic peaks of crystallization at different cooling rates; data for calculation of the CRR length; and measured specific heat capacity curves for PLA/AS blends, prior to accounting for the AS contribution (PDF)

AUTHOR INFORMATION

Corresponding Author

Christine Moresoli − *Department of Chemical Engineering, University of Waterloo, Waterloo N2L 3G1 Ontario, Canada*; Phone: +1 (519) 888-4567ext.35254; Email: cmoresol@uwaterloo.ca

Authors

Rasool Nasseri − *Department of Chemical Engineering, University of Waterloo, Waterloo N2L 3G1 Ontario, Canada*; orcid.org/0000-0003-2140-1359

Aiping Yu − *Department of Chemical Engineering, University of Waterloo, Waterloo N2L 3G1 Ontario, Canada; Waterloo Institute for Nanotechnology, University of Waterloo, Waterloo N2L 3G1 Ontario, Canada*; orcid.org/0000-0002-7422-7537

Zhongshun Yuan − *Institute for Chemicals and Fuels from Alternative Resources, Department of Chemical & Biochemical Engineering, Western University, London N6A 5B9 Ontario, Canada*

Chunbao Charles Xu − *Institute for Chemicals and Fuels from Alternative Resources, Department of Chemical & Biochemical Engineering, Western University, London N6A 5B9 Ontario, Canada*; orcid.org/0000-0001-6543-3817

Complete contact information is available at: https://pubs.acs.org/10.1021/acsomega.2c00360

Notes

The authors declare no competing financial interest.

ACKNOWLEDGMENTS

The authors would like to gratefully acknowledge the OMAFRA New Directions Program (2013−2016) for funding this study. Furthermore, Dr. A. Rahman (University of Waterloo) is also thankfully acknowledged for providing some technical assistance with SAXS experiment.

REFERENCES

(1) Ferri, J. M.; Garcia-Garcia, D.; Sánchez-Nacher, L.; Fenollar, O.; Balart, R. The effect of maleinized linseed oil (MLO) on mechanical performance of poly(lactic acid)-thermoplastic starch (PLA-TPS) blends. *Carbohydr. Polym.* **2016**, *147*, 60−68.

(2) Zuo, Y.; Gu, J.; Yang, L.; Qiao, Z.; Tan, H.; Zhang, Y. Preparation and characterization of dry method esterified starch/polylactic acid composite materials. *Int. J. Biol. Macromol.* **2014**, *64*, 174−180.

(3) Wang, C.; Pan, Z.; Wu, M.; Zhao, P. Effect of reaction conditions on grafting ratio and properties of starch nanocrystals-g-polystyrene. *J. Appl. Polym. Sci.* **2014**, *131*, 40571.

(4) Orford, P. D.; Parker, R.; Ring, S. G.; Smith, A. C. Effect of water as a diluent on the glass transition behaviour of malto-oligosaccharides, amylose and amylopectin. *Int. J. Biol. Macromol.* **1989**, *11*, 91−96.

(5) Zhang, J.-F.; Sun, X. Mechanical Properties of Poly(lactic acid)/Starch Composites Compatibilized by Maleic Anhydride. *Biomacromolecules* **2004**, *5*, 1446−1451.

(6) Xiong, Z.; Yang, Y.; Feng, J.; Zhang, X.; Zhang, C.; Tang, Z.; Zhu, J. Preparation and characterization of poly(lactic acid)/starch composites toughened with epoxidized soybean oil. *Carbohydr. Polym.* **2013**, *92*, 810−816.

(7) Jariyasakoolroj, P.; Chirachanchai, S. Silane modified starch for compatible reactive blend with poly(lactic acid). *Carbohydr. Polym.* **2014**, *106*, 255−263.

(8) Wokadala, O. C.; Emmambux, N. M.; Ray, S. S. Inducing PLA/starch compatibility through butyl-etherification of waxy and high amylose starch. *Carbohydr. Polym.* **2014**, *112*, 216−224.
(9) Fringant, C.; Desbrières, J.; Rinaudo, M. Physical properties of acetylated starch-based materials: Relation with their molecular characteristics. *Polymer* **1996**, *37*, 2663−2673.
(10) Ashogbon, A. O.; Akintayo, E. T. Recent trend in the physical and chemical modification of starches from different botanical sources: A review. *Starch* **2014**, *66*, 41−57.
(11) Nasseri, R.; Ngunjiri, R.; Moresoli, C.; Yu, A.; Yuan, Z.; Xu, C. Poly(lactic acid)/acetylated starch blends: Effect of starch acetylation on the material properties. *Carbohydr. Polym.* **2020**, *229*, 115453.
(12) Saeidlou, S.; Huneault, M. A.; Li, H.; Park, C. B. Poly(lactic acid) crystallization. *Prog. Polym. Sci.* **2012**, *37*, 1657−1677.
(13) Bussiere, P. O.; Therias, S.; Gardette, J.-L.; Murariu, M.; Dubois, P.; Baba, M. Effect of ZnO nanofillers treated with triethoxy caprylylsilane on the isothermal and non-isothermal crystallization of poly(lactic acid). *Phys. Chem. Chem. Phys.* **2012**, *14*, 12301−12308.
(14) Cai, J.; Liu, M.; Wang, L.; Yao, K.; Li, S.; Xiong, H. Isothermal crystallization kinetics of thermoplastic starch/poly(lactic acid) composites. *Carbohydr. Polym.* **2011**, *86*, 941−947.
(15) Li, S.; Xiong, Z.; Fei, P.; Cai, J.; Xiong, H.; Tan, J.; Yu, Y. Parameters characterizing the kinetics of the nonisothermal crystallization of thermoplastic starch/poly(lactic acid) composites as determined by differential scanning calorimetry. *J. Appl. Polym. Sci.* **2013**, *129*, 3566−3573.
(16) Huang, J.; Zhou, J.; Liu, M. Interphase in Polymer Nanocomposites. *JACS Au* **2022**, *2*, 280−291.
(17) Xu, J.; Liu, Z.; Lan, Y.; Zuo, B.; Wang, X.; Yang, J.; Zhang, W.; Hu, W. Mobility Gradient of Poly(ethylene terephthalate) Chains near a Substrate Scaled by the Thickness of the Adsorbed Layer. *Macromolecules* **2017**, *50*, 6804−6812.
(18) Liang, Y.-Y.; Xu, J.-Z.; Liu, X.-Y.; Zhong, G.-J.; Li, Z.-M. Role of surface chemical groups on carbon nanotubes in nucleation for polymer crystallization: Interfacial interaction and steric effect. *Polymer* **2013**, *54*, 6479−6488.
(19) Klonos, P. A.; Papadopoulos, L.; Papageorgiou, G. Z.; Kyritsis, A.; Pissis, P.; Bikiaris, D. N. Interfacial Interactions, Crystallization, and Molecular Dynamics of Renewable Poly(Propylene Furanoate) In Situ Filled with Initial and Surface Functionalized Carbon Nanotubes and Graphene Oxide. *J. Phys. Chem. C* **2020**, *124*, 10220−10234.
(20) Wu, S.; Wang, B.; Xu, X.; Wu, C.; Hu, T.; Zheng, X.; Gong, X. Crystallization behavior and isothermal crystallization kinetics of polylactide/polystyrene-b-polybutadiene-b-polystyrene blends compatibilized with poly(styrene-ran-methyl acrylate). *J. Appl. Polym. Sci.* **2021**, *138*, 50933.
(21) Solarski, S.; Ferreira, M.; Devaux, E. Characterization of the thermal properties of PLA fibers by modulated differential scanning calorimetry. *Polymer* **2005**, *46*, 11187−11192.
(22) Iannace, S.; Nicolais, L. Isothermal crystallization and chain mobility of poly(L-lactide). *J. Appl. Polym. Sci.* **1997**, *64*, 911−919.
(23) Battegazzore, D.; Alongi, J.; Frache, A. Poly (lactic acid)-based composites containing natural fillers: thermal, mechanical and barrier properties. *J. Polym. Environ.* **2014**, *22*, 88−98.
(24) Weyer, S.; Hensel, A.; Schick, C. Temperature Modulated CalorimetryPhase angle correction for TMDSC in the glass-transition region. *Thermochim. Acta* **1997**, *304*−*305*, 267−275.
(25) Gumus, S.; Ozkoc, G.; Aytac, A. Plasticized and unplasticized PLA/organoclay nanocomposites: Short- and long-term thermal properties, morphology, and nonisothermal crystallization behavior. *J. Appl. Polym. Sci.* **2012**, *123*, 2837−2848.
(26) Papageorgiou, G. Z.; Achilias, D. S.; Bikiaris, D. N.; Karayannidis, G. P. Crystallization kinetics and nucleation activity of filler in polypropylene/surface-treated SiO2 nanocomposites. *Thermochim. Acta* **2005**, *427*, 117−128.
(27) Sarikhani, K.; Nasseri, R.; Lotocki, V.; Thompson, R. B.; Park, C. B.; Chen, P. Effect of well-dispersed surface-modified silica nanoparticles on crystallization behavior of poly (lactic acid) under compressed carbon dioxide. *Polymer* **2016**, *98*, 100−109.
(28) Kim, M. S.; Kim, J. C.; Kim, Y. H. Effects of take-up speed on the structure and properties of melt-spun poly(L-lactic acid) fibers. *Polym. Adv. Technol.* **2008**, *19*, 748−755.
(29) Kawai, T.; Rahman, N.; Matsuba, G.; Nishida, K.; Kanaya, T.; Nakano, M.; Okamoto, H.; Kawada, J.; Usuki, A.; Honma, N.; Nakajima, K.; Matsuda, M. Crystallization and Melting Behavior of Poly (l-lactic Acid). *Macromolecules* **2007**, *40*, 9463−9469.
(30) Wu, D.; Xu, H.; Hakkarainen, M. From starch to polylactide and nano-graphene oxide: fully starch derived high performance composites. *RSC Adv.* **2016**, *6*, 54336−54345.
(31) Wokadala, O. C.; Ray, S. S.; Bandyopadhyay, J.; Wesley-Smith, J.; Emmambux, N. M. Morphology, thermal properties and crystallization kinetics of ternary blends of the polylactide and starch biopolymers and nanoclay: The role of nanoclay hydrophobicity. *Polymer* **2015**, *71*, 82−92.
(32) Jeziorny, A. Parameters characterizing the kinetics of the non-isothermal crystallization of poly(ethylene terephthalate) determined by d.s.c. *Polymer* **1978**, *19*, 1142−1144.
(33) Vyazovkin, S.; Sbirrazzuoli, N. Isoconversional Analysis of Calorimetric Data on Nonisothermal Crystallization of a Polymer Melt. *J. Phys. Chem. B* **2003**, *107*, 882−888.
(34) Dobreva, A.; Gutzow, I. Kinetics of Non-isothermal Overall Crystallization in Polymer Melts. *Cryst. Res. Technol.* **1991**, *26*, 863−874.
(35) Helfand, E.; Tagami, Y. Theory of the Interface Between Immiscible Polymers. *J. Chem. Phys.* **1972**, *57*, 1812−1813.
(36) Helfand, E.; Tagami, Y. Theory of the Interface between Immiscible Polymers. II. *J. Chem. Phys.* **1972**, *56*, 3592−3601.
(37) Helfand, E.; Sapse, A. M. Theory of unsymmetric polymer−polymer interfaces. *J. Chem. Phys.* **1975**, *62*, 1327−1331.
(38) Helfand, E. Theory of inhomogeneous polymers: Fundamentals of the Gaussian random-walk model. *J. Chem. Phys.* **1975**, *62*, 999−1005.
(39) Broseta, D.; Fredrickson, G. H.; Helfand, E.; Leibler, L. Molecular weight and polydispersity effects at polymer-polymer interfaces. *Macromolecules* **1990**, *23*, 132−139.
(40) Kong, X.; Silveira, M. D. L. V.; Zhao, L.; Choi, P. A Pseudo Equation-of-State Approach for the Estimation of Solubility Parameters of Polyethylene by Inverse Gas Chromatography. *Macromolecules* **2002**, *35*, 8586−8590.
(41) Ruzette, A.-V. G.; Mayes, A. M. A Simple Free Energy Model for Weakly Interacting Polymer Blends. *Macromolecules* **2001**, *34*, 1894−1907.
(42) Mohanty, A. K.; Misra, M.; Drzal, L. T. *Natural Fibers, Biopolymers, and Biocomposites*; CRC Press, 2005.
(43) Agrawal, A.; Saran, A. D.; Rath, S. S.; Khanna, A. Constrained nonlinear optimization for solubility parameters of poly(lactic acid) and poly(glycolic acid)—validation and comparison. *Polymer* **2004**, *45*, 8603−8612.
(44) Cheng, B.; Qian, L.; Qian, H.-j.; Lu, Z.-y.; Cui, S. Effects of stereo-regularity on the single-chain mechanics of polylactic acid and its implications on the physical properties of bulk materials. *Nanoscale* **2017**, *9*, 14312−14316.
(45) Nakanishi, Y.; Norisuye, T.; Teramoto, A.; Kitamura, S. Conformation of amylose in dimethyl sulfoxide. *Macromolecules* **1993**, *26*, 4220−4225.
(46) Norisuye, T. Viscosity Behavior and Conformation of Amylose in Various Solvents. *Polym. J.* **1994**, *26*, 1303−1307.
(47) Cheung, Y. W.; Stein, R. S.; Lin, J. S.; Wignall, G. D. Small-Angle Scattering Investigations of Poly(.epsilon.-caprolactone)/Polycarbonate Blends. 2. Small-Angle X-ray and Light Scattering Study of Semicrystalline/Semicrystalline and Semicrystalline/Amorphous Blend Morphologies. *Macromolecules* **1994**, *27*, 2520−2528.
(48) Vonk, C. G. Investigation of non-ideal two-phase polymer structures by small-angle X-ray scattering. *J. Appl. Crystallogr.* **1973**, *6*, 81−86.
(49) Ruland, W. Small-angle scattering of two-phase systems: determination and significance of systematic deviations from Porod's law. *J. Appl. Crystallogr.* **1971**, *4*, 70−73.

https://doi.org/10.1021/acsomega.2c00360
ACS Omega 2022, 7, 27851−27863

(50) Donth, E. The size of cooperatively rearranging regions at the glass transition. *J. Non-Cryst. Solids* **1982**, *53*, 325−330.
(51) Carrillo, J.-M. Y.; Cheng, S.; Kumar, R.; Goswami, M.; Sokolov, A. P.; Sumpter, B. G. Untangling the Effects of Chain Rigidity on the Structure and Dynamics of Strongly Adsorbed Polymer Melts. *Macromolecules* **2015**, *48*, 4207−4219.
(52) Simmons, D. S. An Emerging Unified View of Dynamic Interphases in Polymers. *Macromol. Chem. Phys.* **2016**, *217*, 137−148.
(53) Cheng, S.; Carroll, B.; Lu, W.; Fan, F.; Carrillo, J.-M. Y.; Martin, H.; Holt, A. P.; Kang, N.-G.; Bocharova, V.; Mays, J. W.; Sumpter, B. G.; Dadmun, M.; Sokolov, A. P. Interfacial Properties of Polymer Nanocomposites: Role of Chain Rigidity and Dynamic Heterogeneity Length Scale. *Macromolecules* **2017**, *50*, 2397−2406.
(54) Holt, A. P.; Griffin, P. J.; Bocharova, V.; Agapov, A. L.; Imel, A. E.; Dadmun, M. D.; Sangoro, J. R.; Sokolov, A. P. Dynamics at the Polymer/Nanoparticle Interface in Poly(2-vinylpyridine)/Silica Nanocomposites. *Macromolecules* **2014**, *47*, 1837−1843.
(55) Sargsyan, A.; Tonoyan, A.; Davtyan, S.; Schick, C. The amount of immobilized polymer in PMMA SiO2 nanocomposites determined from calorimetric data. *Eur. Polym. J.* **2007**, *43*, 3113−3127.
(56) Liu, Y.; Hamon, A.-L.; Haghi-Ashtiani, P.; Reiss, T.; Fan, B.; He, D.; Bai, J. Quantitative Study of Interface/Interphase in Epoxy/Graphene-Based Nanocomposites by Combining STEM and EELS. *ACS Appl. Mater. Interfaces* **2016**, *8*, 34151−34158.
(57) Katiyar, V.; Nanavati, H. Ring-opening polymerization of L-lactide using N-heterocyclic molecules: mechanistic, kinetics and DFT studies. *Polym. Chem.* **2010**, *1*, 1491−1500.
(58) Strobl, G. R.; Schneider, M. Direct evaluation of the electron density correlation function of partially crystalline polymers. *J. Polym. Sci., Polym. Phys. Ed.* **1980**, *18*, 1343−1359.
(59) Park, J. W.; Im, S. S. Miscibility and morphology in blends of poly(l-lactic acid) and poly(vinyl acetate-co-vinyl alcohol). *Polymer* **2003**, *44*, 4341−4354.

https://doi.org/10.1021/acsomega.2c00360
ACS Omega 2022, 7, 27851−27863